Thermometry and up-conversion luminescence of Ln^{3+} (Ln = Er, Ho, Tm)-doped double molybdate $LiYbMo_2O_8$

Xiangyan Yun[1], Jun Zhou[1], Yaohui Zhu[1], Maxim S. Molokeev[2,3,4], Yetong Jia[1], Chao Wei[1], Denghui Xu[1,*] (ORCID), and Jiayue Sun[1]

[1] *School of Science, Beijing Technology and Business University, Beijing 100048, China*
[2] *Laboratory of Crystal Physics, Kirensky Institute of Physics, Federal Research Center KSC SB RAS, Krasnoyarsk, Russia 660036*
[3] *Siberian Federal University, Krasnoyarsk, Russia 660041*
[4] *Department of Physics, Far Eastern State Transport University, Khabarovsk, Russia 680021*

ABSTRACT

The discovery of stable and highly sensitive up-conversion (UC) phosphors using the fluorescence intensity ratio (FIR) is a significant challenge in the field of optical temperature sensor. $Er^{3+}/Ho^{3+}/Tm^{3+}$-doped $LiYbMo_2O_8$ UC phosphors with excellent luminescence properties were successfully synthesized through a high-temperature solid-state reaction, and the crystal structure and UC luminescence properties were discussed in detail. The UC process has been investigated by spectra pump power dependence and further explained via the energy level diagram. All emission processes about Er^{3+} ions and Ho^{3+} ions are two-photon processes and the blue emission process about Tm^{3+} ions is a combination of two-photon process and three-photon process. Thermal sensing performances depended on FIR technology were estimated and the sensitivities of $LiYb_{1-x}Mo2O8:xLn^{3+}$ included absolute sensitivity (S_a) and relative sensitivity (S_r) can produce particular change rules with the temperature, which can serve as excellent candidates for applications in optical temperature sensing. With the increase of temperature, the maximum values of S_r of $LiYb_{1-x}Mo_2O_8:xLn^{3+}$ are 1.16% K^{-1} ($0.05Er^{3+}$), 0.25% K^{-1} ($0.01Ho^{3+}$), and 0.51% K^{-1} ($0.01Tm^{3+}$), respectively. In addition, the S_a value of $LiYb_{0.95}Mo_2O_8:0.05Er^{3+}$ phosphor will reach the maximum (1.08% K^{-1}) at 475 K, while the maximum values of S_a of $LiYb_{0.99}Mo_2O_8:0.01Ho^{3+}$ and $LiYb_{0.99}Mo_2O_8:0.01Tm^{3+}$ are 0.16% K^{-1}, 0.14% K^{-1}.

1 Introduction

Recently, lanthanide (Ln^{3+})-doped up-conversion (UC) phosphors have attracted substantial attention because of their promising applications in solar cells, bioimaging, color display, sensor techniques, and so on [1, 2]. Among these Ln^{3+} ions, Yb^{3+} ions typically have employed as sensitizers in the UC process due to a large absorption cross-section in the near infrared (NIR) region than many other lanthanide elements with similar energy levels and only one excited state, which can be easily excited by 980 nm [3, 4]. And it is always co-doped with activator ions (Er^{3+}, Ho^{3+} and Tm^{3+}) to produce strong red, green, blue, and NIR UC emissions [5].

As is well known, temperature is one of the effective parameters in the field of industry, medicine, and other scientific research [6]. As a popular technology in temperature sensing, fluorescence intensity ratio (FIR) is based on the measurement of emission intensities from two thermally coupled level with the temperature [7]. Furthermore, FIR technology can be used to provide more accurate long-distance temperature measurements because it is independent of the frequency spectrum. In addition, if a luminescent material has high sensitivity, it can be qualified to act as a temperature sensor [8]. Recently, optical temperature sensors based on rare earth activated up-conversion (UC) phosphor have been widely concerned, such as $Gd_2TiO_5:Yb^{3+}/Er^{3+}$, [9] $KLu(WO_4)_2:Yb^{3+}/Ho^{3+}$, [10] and $KY(MoO_4)_2:Yb^{3+}/Er^{3+}/Ho^{3+}/Tm^{3+}$ [11] phosphors. These results definitely indicated that Ln^{3+} ($Ln = Er^{3+}/Ho^{3+}/Tm^{3+}$) ions-doped inorganic phosphors with excellent properties have been expected to be used in optical temperature sensing.

It is well known that a suitable host for efficient UC phosphors should have a low phonon energy [12]. Among these UC materials, Ln^{3+}-doped double molybdates are regarded as a fascinating inorganic functional material, not only because of their low phonon energy, but owing to their large lanthanide admittance [13]. Among molybdates, the double molybdate structure matrix is considered as a potential host material because of its chemical stabilities and excellent thermal properties. Among them, $LiYbMo_2O_8$ was first described by Zaldo et al., which has a monoclinic structure with a space group of $I4_1/a$ [14]. Since the host material possesses heavy metal elements, such as Yb and Mo elements, the host

material has lower lattice vibration energy [15, 16]. Thus, nonradiative transition rates between energy levels of rare earth ions would be low. And one of the biggest characteristics of this research is that the $LiYbMo_2O_8:Ln^{3+}$ phosphors used Yb^{3+} ions, which has the capacity to accommodate higher content of rare earth ions, because the Yb^{3+} ion is commonly used as a favorable sensitizer [1]. However, to the best of our knowledge, the application of $Er^{3+}/Ho^{3+}/Tm^{3+}$-doped $LiYbMo_2O_8$ UC phosphors in temperature sensing has not been reported so far. Herein, we have demonstrated a series of $LiYb_{1-x}Mo_2O_8:xLn^{3+}$ ($Ln^{3+} = Er^{3+}/Ho^{3+}/Tm^{3+}$) phosphors, and UC luminescence properties for temperature sensing were investigated in detail, which have high performance in the field of temperature sensing based on the FIR technology.

2 Experimental section

2.1 Materials and preparation

All the chemicals were commercially purchased from Aladdin and used without further purification. A series of Ln ($Ln = Er^{3+}/Ho^{3+}/Tm^{3+}$)-doped $LiYbMo_2O_8$ samples were synthesized by a conventional high-temperature solid-state reaction starting from a mixture containing Li_2CO_3 (A.R.), Yb_2O_3 (99.99%), MoO_3 (99.99%), Er_2O_3 (99.99%), Ho_2O_3 (99.99%), and Tm_2O_3 (99.99%) at the specified stoichiometric ratio. After grinding, a homogeneous mixture of several samples was placed into an alumina crucible and then sintered in air at 800 °C for 10 h. Finally, the as-synthesized samples were slowly cooled to room temperature, and ground again to obtain the $LiYb_{1-x}Mo_2O_8:xLn^{3+}$ fluorescent phosphors.

2.2 Measurements and characterization

The powder X-ray diffraction (XRD) patterns of $LiYb_{1-x}Mo_2O_8:xLn^{3+}$ samples were examined with a Germanic model D2 PHASER (Bruker, Karlsruhe) using CuKα radiation ($\lambda = 0.1506$ Å), which was operated at 30 kV and 10 mA. The powder diffraction pattern for Rietveld analysis was collected with the same diffractometer. The step size of 2θ was 0.016°, and the counting time was 1 s per step. Rietveld refinement was performed by using TOPAS 4.2

software [17]. The room-temperature UC emission spectra (PL) were recorded by a FLSP9200 fluorescence spectrophotometer (Edinburgh Instruments Ltd., U.K.) with the output of a 980 nm laser. Temperature-dependent UC PL spectra were measured by FLS920 connected with a heating equipment.

3 Results and discussions

3.1 Phase structure of $LiYb_{1-x}Mo_2O_8:xLn^{3+}$ samples

Figure 1a displays the observed (black), calculated (red), and the difference (gray) XRD profiles for the Rietveld refinement of $LiYbMo_2O_8$. It is found that the $LiYbMo_2O_8$ phase crystallizes as a monoclinic structure with a space group of $I4_1/a$ and lattice constants of $a = 11.0989$ (2) Å, $c = 19.3907$ (2) Å, $V = 290.387$ (7) Å^3, and $Z = 2$, which are close to $LiLu(MoO_4)_2$ [18]. Site of Lu ion was occupied by Yb ion (Fig. 1a). Moreover, the refinement was stable and gave low R-factors (Table 1). Coordinates of atoms and main bond lengths are in Table 2 and Table 3, respectively. A visualization of the $LiYbMo_2O_8$ structure is presented in the inset of Fig. 1a. In the $LiYbMo_2O_8$ crystal structure, the four oxygen atoms surround the Mo^{6+} ions to form an isolated $[MoO_4]^{2-}$ tetrahedron, while the cations of Li^+ and Yb^{3+} are arbitrarily distributed among the isolated $[MoO_4]^{2-}$ tetrahedra. The XRD patterns of the as-synthesized $LiYb_{0.95}Mo_2O_8:0.05\ Ln^{3+}$ (Ln = Er, Ho, Tm) samples and undoped $LiYbMo_2O_8$ phosphors are shown in Fig. 1b. It can be found that all the diffraction peaks can be exactly indexed by the

**Table 1** Main parameters of processing and refinement of the $LiYb(MoO_4)_2$ sample

Compound	$LiYb(MoO_4)_2$
Sp.Gr.	5.11504 (5)
a, Å	11.0989 (2)
c, Å	19.3907 (2)
V, Å^3	290.387 (7)
Z	2
2θ-interval, °	8–120
R_{wp}, %	6.43
R_p, %	4.97
R_{exp}, %	2.60
χ^2	2.48
R_B, %	1.77

Table 2 Fractional atomic coordinates and isotropic displacement parameters (Å^2) of $LiYb(MoO_4)_2$

Atom	x	Y	z	B_{iso}	Occ.
Li	0	0.25	0.625	0.90 (9)	0.5
Yb	0	0.25	0.625	0.90 (9)	0.5
Mo	0	0.25	0.125	1.17 (10)	1
O	0.2433 (12)	0.0906 (8)	0.0404 (3)	1.60 (16)	1

corresponding standard data for trigonal phase of $LiYbMo_2O_8$ (ICSD 152282), suggesting that doped Ln^{3+} have been successfully dissolved in the $LiYbMo_2O_8$ host lattice [19]. On the basis of the similar ion radius (Yb^{3+}: $R = 0.985$ Å, Er^{3+}: $R = 1.004$ Å, Ho^{3+}: $R = 1.015$ Å, Tm^{3+}: $R = 0.994$ Å, coordination number = 8) and valence, it can be approximately assumed that Ln^{3+} (Ln = Er, Ho, Tm) ion dopants were expected to occupy the Yb^{3+} sites in the $LiYbMo_2O_8$ host.
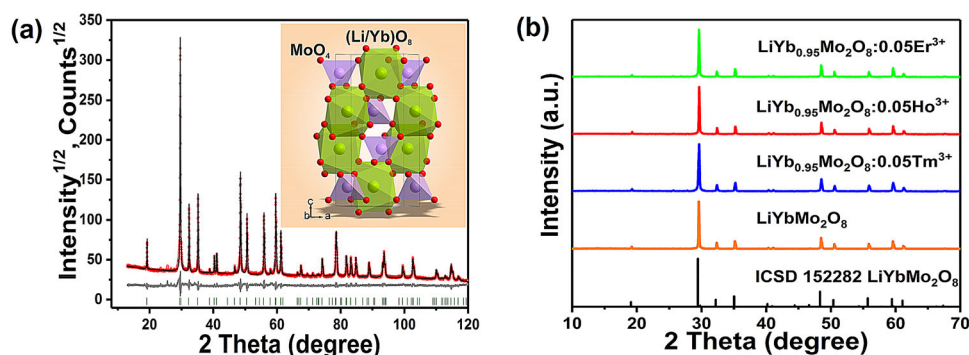
Fig. 1 a Rietveld structure refinement XRD pattern of $LiYbMo_2O_8$ phosphor. The inset presents the crystal structure of $LiYbMo_2O_8$. **b** XRD patterns of $LiYbMo_2O_8$, $LiYb_{0.95}Mo_2O_8:0.05Er^{3+}$, $LiYb_{0.95}Mo_2O_8:0.05Ho^{3+}$, $LiYb_{0.95}Mo_2O_8:0.05Tm^{3+}$, and ICSD 152282 as a comparison

Table 3 Main bond lengths (Å) of LiYb(MoO$_4$)$_2$

(Yb/Li)—O^i	2.375 (5)	Mo—O	1.760 (5)
(Yb/Li)—O^{ii}	2.400 (5)		
Symmetry codes: (i) $- x + 1/2, - y, z + 1/2$; (ii) $- x + 1/2, - y + 1/2, - z + 1/2$			

3.2 Luminescence properties of LiYb$_{1-x}$Mo$_2$O$_8$:xLn^{3+} samples

In the LiYbMo$_2$O$_8$ host rich in sensitizers, Yb^{3+} ions not only contribute to the formation of crystal structure, but also act as sensitizers in the UC process [20]. Figure 2 shows the UC emission spectra of LiYb$_{1-x}$-Mo$_2$O$_8$:xLn^{3+} powder with different concentrations of Ln^{3+} ions under 980 nm excitation. As shown in Fig. 2a, LiYb$_{1-x}$Mo$_2$O$_8$:xEr^{3+} ($x = 0.005$, 0.01, 0.03, 0.05, 0.10, 0.15, 0.25) samples show intense green emission bands (524 nm and 545 nm) and a negligible weak red emission (657 nm and 672 nm), which corresponds to the transitions of $^2H_{11/2} \rightarrow {}^4I_{15/2}$, $^4S_{3/2} \rightarrow {}^4I_{15/2}$, $^4F_{9/2(2)} \rightarrow {}^4I_{15/2}$, and $^4F_{9/2(1)} \rightarrow {}^4I_{15/2}$,

respectively [21]. Besides, the green emission and weak red emission intensity increased gradually with the increase of Er^{3+} content and reached a maximum when the concentration of Er^{3+} was 0.05. The inset of Fig. 2a gives the $^4S_{3/2} \rightarrow {}^4I_{15/2}$ (553 nm) emission intensity as a function of Er^{3+} concentration, which reveals that the sample for $x = 0.05$ exhibits the strongest emission intensity due to the concentration quenching effect.

If the average distance between the same Er^{3+} ions is too large to hinder the energy transfer, the concentration quenching phenomena will not occur [22]. Thus the critical distance (R_c) should be estimated which is to better understand the associated concentration quenching phenomenon and the linked
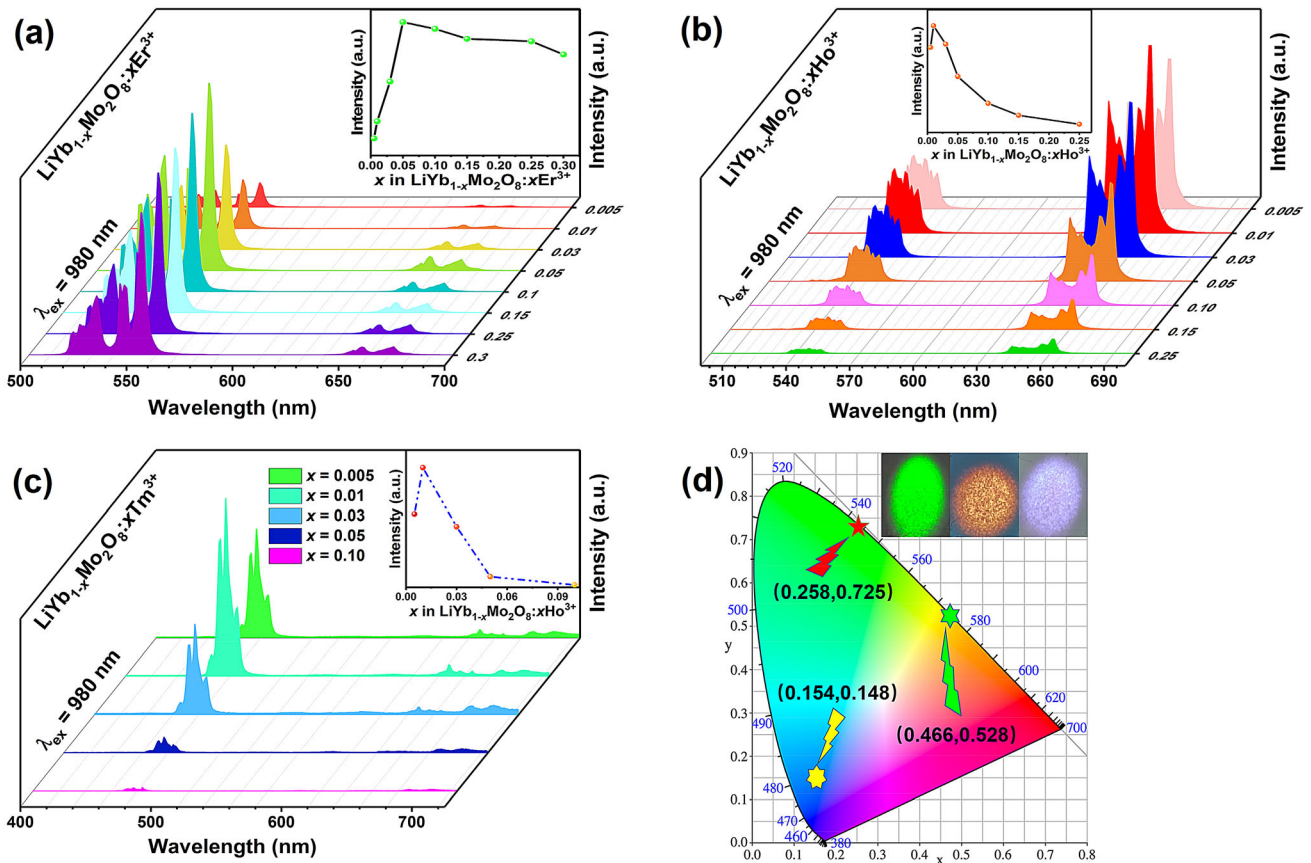
Fig. 2 The UC spectra of **a** LiYb$_{1-x}$Mo$_2$O$_8$:xEr^{3+}, **b** LiYb$_{1-x}$Mo$_2$O$_8$:xHo^{3+}, and **c** LiYb$_{1-x}$Mo$_2$O$_8$:xTm^{3+} samples. The insets show the variation of the emission intensities. **d** The chromaticity diagram of LiYb$_{0.95}$Mo$_2$O$_8$:0.05Er^{3+}, LiYb$_{0.99}$Mo$_2$O$_8$:0.01Ho^{3+}, and LiYb$_{0.99}$Mo$_2$O$_8$:0.01Tm^{3+} samples excited at 980 nm

energy transfer mechanism. The critical distance (R_c) must be approximately calculated using the following function given by Blasse [23]:

$$R_c \approx 2\left[\frac{3V}{4\pi x_c N}\right]^{1/3},\qquad(1)$$

where x_c is the critical concentration ($x_c = 0.05$), V shows the exact volume of the host cell ($V = 291.11$ Å^3), and N represents the number of obtainable sites for the Er^{3+} ions in a unit cell ($N = 8$). After calculation, the value of R_c is 11.16 Å which is greater than 5 Å, indicating little possibility of energy transfer via the exchange interaction mechanism. Figure 2b shows the emission spectra of LiYb$_{1-x}$Mo$_2$O$_8$:xHo^{3+} under 980 nm excitation. It is found that the PL spectra have similar spectral profiles, except for the emission intensities. The emission peaks centered at about 547 nm and 662 nm are ascribed to the $^5F_4 \rightarrow {}^5I_8$, $^5S_2 \rightarrow {}^5I_8$, and $^5F_5 \rightarrow {}^5I_8$ transitions of Ho^{3+} ions, respectively, and the transition of $^5F_5 \rightarrow {}^5I_8$ at 662 nm exhibits the comparative high intensity. In addition, as seen from the inset of Fig. 2b, the optimal doping concentration was determined as 0.01 and the intensity declines dramatically when the concentration of Ho^{3+} exceeds 1 mol% owing to the concentration quenching. Figure 2c illustrates the emission spectra of LiYb$_{1-x}$Mo$_2$O$_8$:xTm^{3+} under 980 nm excitation, which are composed of a blue emission region and a faint emission region. The emission peaks located at 477 nm, 486 nm, 649 nm, and 688 nm are owing to the transitions of $^1G_{4(2)} \rightarrow {}^3H_6$, $^1G_{4(1)} \rightarrow {}^3H_6$, $^1G_{4(1)} \rightarrow {}^3F_4$, and $^3F_{2,3} \rightarrow {}^3H_6$, respectively [15], and the intensity can reach the maximum when the concentration of Tm^{3+} is 0.01. Besides, the R_c of the prepared LiYb$_{0.99}$Mo$_2$O$_8$:0.01Ho^{3+} and LiYb$_{0.99}$Mo$_2$O$_8$:0.01Tm^{3+} samples are 19.08 Å, which are marginally greater than that of LiYb$_{0.95}$Mo$_2$O$_8$:0.05Er^{3+}. The corresponding CIE coordinates for the LiYb$_{0.95}$Mo$_2$O$_8$:0.05Er^{3+}, LiYb$_{0.99}$Mo$_2$O$_8$:0.01Ho^{3+}, and LiYb$_{0.99}$Mo$_2$O$_8$:0.01Tm^{3+} samples and the digital images excited at 980 nm are shown in Fig. 2d, which are (0.258, 0.725), (0.466, 0.528), and (0.154, 0.148), respectively. It is worth mentioning that the CIE coordinates of LiYb$_{0.95}$Mo$_2$O$_8$:0.05Er^{3+}, LiYb$_{0.99}$Mo$_2$O$_8$:0.01Ho^{3+} are adjacent to the edge of the curve, indicating the high color saturation [24].

3.3 UC mechanisms

In order to understand the UC luminescence mechanisms, the variation of the emission intensities excited at 980 nm as a function of the pump power were tested and shown in Fig. 3. As shown in Fig. 3, all the observed luminous intensity patterns of LiYb$_{0.95}$Mo$_2$O$_8$:0.05Ln^{3+} samples are enhanced with increasing the excitation power. In general, the dependence of the output UC luminescent intensity (I) on the infrared pump power (P) can be approximately expressed as follows [25]:

$$I \propto KP^n,\qquad(2)$$

where K is the co-efficient related to the material, P is the pump power, and n is the number of total photons needed to produce UC luminescence, which can be simply appraised from the slopes of the linear fit [26]. The inset of Fig. 3a shows the Ln–Ln plot of the integrated green and red emission intensity as a function of the excitation power for the as-studied LiYb$_{0.95}$Mo$_2$O$_8$:0.05Er^{3+} sample. The amount of photons n is calculated to be around 1.500 and 1.546, respectively, which indicates that both two-photon processes are responsible for the green and red UC emissions for the as-studied LiYb$_{0.95}$Mo$_2$O$_8$:0.05Er^{3+} phosphor [27]. Similarly, the calculated n for the $^5S_2 \rightarrow {}^5I_8$, $^5F_5 \rightarrow {}^5I_8$ processes in the LiYb$_{0.95}$Mo$_2$O$_8$:0.05Ho^{3+} and the $^1G_{4(2)} \rightarrow {}^3H_6$, $^1G_{4(1)} \rightarrow {}^3H_6$ processes of LiYb$_{0.95}$Mo$_2$O$_8$:0.05Tm^{3+} are 1.506, 1.623, 1.979, and 2.281, respectively, which shows that all emission processes about Ho^{3+} ions are two-photon processes and the blue emission process about Tm^{3+} ions is a combination of two-photon process and three-photon process, as shown in the inset of Fig. 3b, c.

To better understand the UC mechanism, the schematic energy level diagram and possible transitions of LiYb$_{1-x}$Mo$_2$O$_8$:xLn^{3+} samples upon 980 nm excitation are proposed as shown in Fig. 3. First of all, the Yb^{3+} and Er^{3+} ion can be effectively excited from the ground state $^2F_{7/2}$ and $^4I_{15/2}$ to the excited states $^2F_{5/2}$ and $^4I_{11/2}$, respectively, which is known as the ground state absorption (GSA): Yb^{3+}($^2F_{7/2}$) + a NIR photon $\rightarrow$ Yb^{3+}($^2F_{5/2}$), Er^{3+}($^4I_{15/2}$) + a NIR photon $\rightarrow$ Er^{3+}($^4I_{11/2}$). Then, the energy of metastable energy level $^4I_{11/2}$ of Er^{3+} ion also comes from the energy transfer (ET) between Yb^{3+} and Er^{3+} ions: Yb^{3+}($^2F_{5/2}$) + Er^{3+}($^4I_{15/2}$) $\rightarrow$ Yb^{3+}($^2F_{7/2}$) + Er^{3+}($^4I_{11/2}$). Subsequently, electrons at the $^4I_{11/2}$
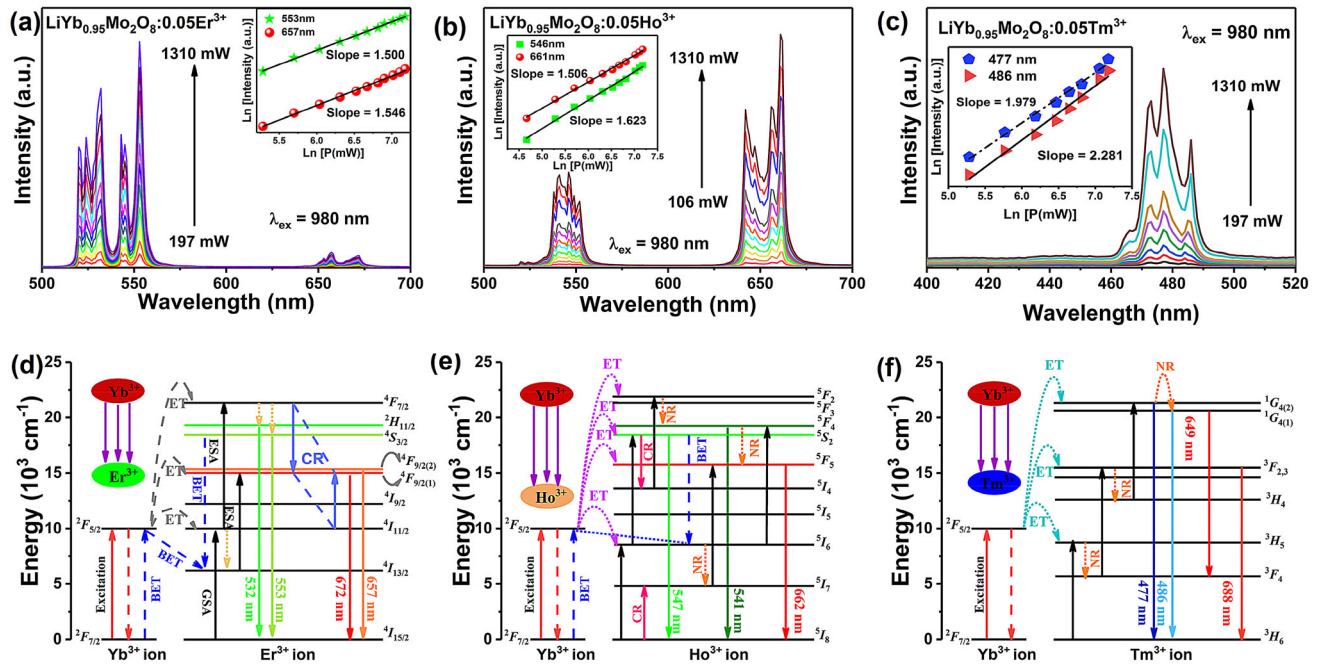
Fig. 3 Visible UC emission spectra of **a** LiYb$_{0.95}$Mo$_2$O$_8$:0.05Er^{3+}, **b** LiYb$_{0.95}$Mo$_2$O$_8$:0.05Ho^{3+}, and **c** LiYb$_{0.95}$Mo$_2$O$_8$:0.05Tm^{3+}. And insets show the pump power dependence of intensities. Schematic energy level chart of Ln^{3+} ion in the LiYbMo$_2$O$_8$ system: **d** Ln^{3+} = Er^{3+} **e** Ln^{3+} = Ho^{3+} **f** Ln^{3+} = Tm^{3+}

level could partly relax to the $^4I_{13/2}$ level by a non-radiative relaxation process. The green emission located at 532 nm and 553 nm corresponding to $^2H_{11/2} \rightarrow ^4I_{15/2}$ and $^4S_{3/2} \rightarrow ^4I_{15/2}$ of Er^{3+} emission originated from the $^4F_{7/2}$ decay nonradiative transition to $^2H_{11/2}$ and $^4S_{3/2}$ [28]. In addition, there are three potential transition modes of Er^{3+} ions from the $^4I_{11/2}$ excited state to the $^4F_{7/2}$ level. The first possible way is to transfer the phonon-assisted energy from $^2F_{5/2}$ excited state of the Yb^{3+} ions to the Er^{3+} ions, which makes Er^{3+} ion transition to the $^4F_{7/2}$ level, thereby prompting the Yb^{3+} ions return to the $^2F_{7/2}$ ground state: Yb^{3+}($^2F_{5/2}$) + Er^{3+}($^4I_{11/2}$) → Yb^{3+}($^2F_{7/2}$) + Er^{3+}($^4F_{7/2}$). The second situation occurs when the Er^{3+} ions in excited state $^4I_{11/2}$ performs excited state absorption (ESA), and the whole process is independent of Yb^{3+}. The last is the energy transfer from the excited state $^4I_{11/2}$ of neighboring Er^{3+} ions, in which two excited Er^{3+} ions interact, with one Er^{3+} ion returning to the ground state and the other ion jumping to the excited state $^4F_{7/2}$: Er^{3+}($^4I_{11/2}$) + Er^{3+}($^4I_{11/2}$) → Er^{3+}($^4I_{15/2}$) + Er^{3+}($^4F_{7/2}$). For the relatively weak red emission in LiYb$_{01-x}$Mo$_2$O$_8$:-xEr^{3+}, the emission levels mainly come from the excited states $^4F_{9/2(2)}$ and $^4F_{9/2(1)}$, which come from three sources. They are the cross-relaxation (CR:

Er^{3+}($^4I_{11/2}$) + Er^{3+}($^4F_{7/2}$) → Er^{3+}($^4F_{9/2}$) + Er^{3+}($^4F_{9/2}$)) between the Er^{3+} ion at the $^4I_{11/2}$ level and $^4F_{7/2}$ state, the back energy transfer (BET), and the ET: Yb^{3+}($^2F_{5/2}$) + Er^{3+}($^4I_{13/2}$) → Yb^{3+}($^2F_{7/2}$) + Er^{3+}($^4F_{9/2}$) between Yb^{3+} and Er^{3+} ions. Figure 3e illustrates the energy level transition diagram of LiYb$_{1-x}$Mo$_2$O$_8$:xHo^{3+}, which should be noted that the ET between Yb^{3+} ion and Ho^{3+} ion must be assisted by phonons. In addition, GSA, ESA, CR, and BET are integrally included in the whole process of visible light emission of UC. The red emission ($^5F_5 \rightarrow ^5I_8$, 662 nm) of Ho^{3+} ions are accomplished via the following processes: Yb^{3+}($^2F_{5/2}$) + Ho^{3+}($^5I_8$) → Yb^{3+}($^2F_{7/2}$) + Ho^{3+}($^5I_6$), Yb^{3+}($^2F_{5/2}$) + Ho^{3+}($^5I_6$) → Yb^{3+}($^2F_{7/2}$) + Ho^{3+}($^5F_4$, $^5S_2$), and Yb^{3+}($^2F_{5/2}$) + Ho^{3+}($^5I_7$) → Yb^{3+}($^2F_{7/2}$) + Ho^{3+}($^5F_5$), where the metastable $^5F_5$ and $^5I_7$ states are populated by nonradiative transition (NR) from $^5S_2$ and $^5I_6$ levels [29]. Certainly, the excited states of $^5I_7$ and $^5I_4$ can be populated through the CR process: Ho^{3+}($^5S_2$) + Ho^{3+}($^5I_8$) → Ho^{3+}($^5I_4$) + Ho^{3+}($^5I_7$) [30]. For the green emission band from $^5F_4 \rightarrow ^5I_8$, $^5S_2 \rightarrow ^5I_8$ process, there are additional sources of $^5F_4/^5S_2$ excited energy state: Yb^{3+}($^2F_{5/2}$) + Ho^{3+}($^5I_4$) → Yb^{3+}($^2F_{7/2}$) + Ho^{3+}($^5F_2$) [31]. Hence, $^5F_2$ level can reach the $^5F_4$, and $^5F_4$ can reach the $^5S_2$ state by nonradiative (NR)

transition. The same UC mechanism applies to $LiYb_{1-x}Mo_2O_8{:}xTm^{3+}$ as presented in Fig. 3f [32, 33]. As a result, the above analysis perfectly matches the actual luminescence of the as-prepared $LiYb_{1-x}Mo_2O_8{:}xLn^{3+}$ phosphors.

3.4 UC thermometric properties and application

In order to investigate the temperature sensing behavior of $LiYbMo_2O_8{:}Ln^{3+}$, the temperature-dependent UC spectra under 980 nm excitation were obtained at different temperatures, as shown in Fig. 4. Except for the emission intensity, the shape and position of emission spectrum are basically unchanged. For $LiYb_{0.99}Mo_2O_8{:}0.01Er^{3+}$ sample as shown in Fig. 4a the emission intensity of 553 nm ($^4S_{3/2} \rightarrow {}^4I_{15/2}$) decreases, while the intensity of 532 nm ($^2H_{11/2} \rightarrow {}^4I_{15/2}$) emission peak generally increases first and then decreases. The enhancement of the 532 nm ($^2H_{11/2} \rightarrow {}^4I_{15/2}$) emission may be related to the thermally coupled effect, for which the partial relaxed electrons in the $^4S_{3/2}$ level can efficiently transition to the $^2H_{11/2}$ level along with the increase of temperature [34]. Nevertheless, the red

emission band composed of two peaks of $LiYb_{0.99}Mo_2O_8{:}0.01Ho^{3+}$ sample assigned to the radiative transition from dissimilar Stark sublevels of $^5F_5$ energy level to the $^5I_8$ energy level represent an unusual thermal evolution, which is related to the intensity of these two peaks (Fig. 4b) [10]. It can be seen that the UC emission intensity of 643 nm ($^5F_5 \rightarrow {}^5I_8$) and 662 nm ($^5F_5 \rightarrow {}^5I_8$) greatly change with the temperature from 300 to 451 K. Furthermore, it can be proved that these two special Stark sublevels (643 nm, 662 nm) are thermally coupled, because the energy gap is little and it causes the upper Stark sublevel to be thermally filled from the lower Stark sublevel along with temperature rising. Similar to Ho^{3+}, the emission peak at 477 nm ($^1G_{4(2)} \rightarrow {}^3H_6$) and 486 nm ($^1G_{4(1)} \rightarrow {}^3H_6$) decreases gradually(Fig. 4c) [35]. The $^1G_{4(1)}$-level and $^1G_{4(2)}$-level of Tm^{3+} ions are also thermally coupled levels which can be analyzed using FIR technology according to the previous relevant literature reports [32, 36]. All the above phenomena indicate that $LiYb_{1-x}Mo_2O_8{:}xLn^{3+}$ have thermal coupling properties, which can be well used in the field of temperature sensor [37].
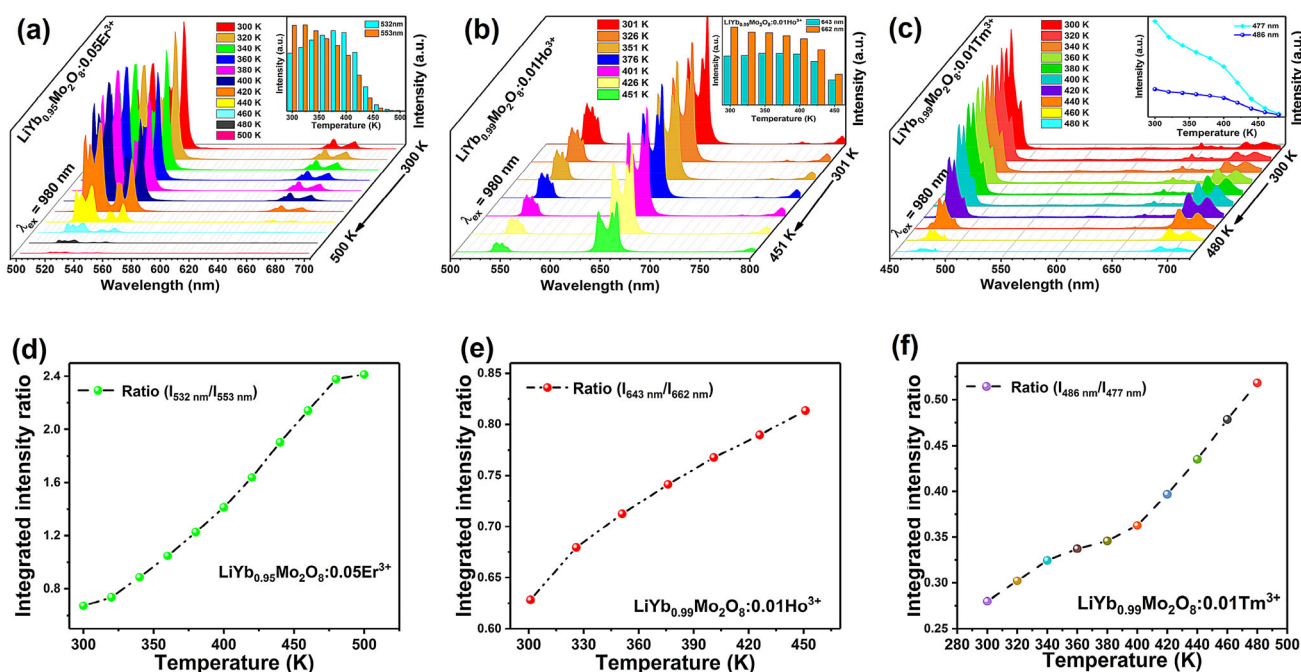
Fig. 4 Relative UC emission intensity of **a** $LiYb_{0.95}Mo_2O_8{:}0.05Er^{3+}$, **b** $LiYb_{0.99}Mo_2O_8{:}0.01Ho^{3+}$, and **c** $LiYb_{0.99}Mo_2O_8{:}0.01Tm^{3+}$ sample under different temperatures. The insets show the variation of emission intensity. Variation of green UC luminescence intensity ratios of **d** $LiYb_{0.95}Mo_2O_8{:}0.05Er^{3+}$, **e** $LiYb_{0.99}Mo_2O_8{:}0.01Ho^{3+}$, and **f** $LiYb_{0.99}Mo_2O_8{:}0.01Tm^{3+}$

As can be seen from Fig. 4d–f, the intensity ratio of $I_{532\ nm}/I_{553\ nm}$, $I_{643\ nm}/I_{662\ nm}$, and $I_{486\ nm}/I_{477\ nm}$ of $LiYb_{1-x}Mo_2O_8:xLn^{3+}$ phosphors are gradually increased, which make it possible to use the relative intensity thorough the technique of FIR. The FIR technology involves measuring the thermal dependence of the fluorescence intensity produced by the thermal coupling of two different electron energy levels and calculating their ratio, which is usually given as follows [38]:

$$FIR = \frac{I_1}{I_2} = B \exp\left(\frac{\Delta E}{K_B T}\right), \qquad (3)$$

where B, ΔE, K_B, and T are the pre-exponential factor, the energy gap between the two states considered, the Boltzmann constant and the absolute temperature, respectively. According to Eq. 3, the ratio of I_1/I_2 is only related to temperature.
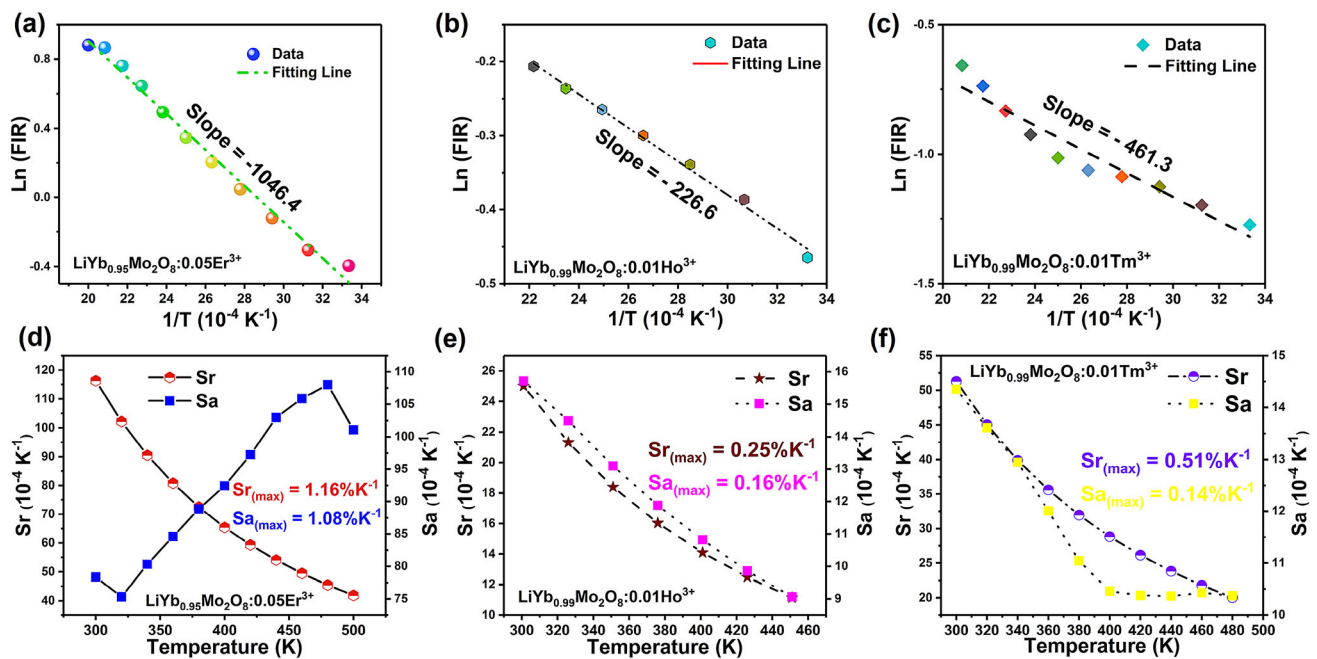
Lognormal plot of the FIR of I_1/I_2 as a function of the reciprocal of temperature about $LiYb_{1-x}Mo_2O_8:xLn^{3+}$ samples are shown in Fig. 5a–c. The slopes of the near-linear curves are, respectively, equal to -1064.4, -226.6, and -461.3, which can represent the numerical of $\Delta E/K$ about three $LiYb_{1-x}Mo_2O_8:xLn^{3+}$ samples [39]. Moreover, the sensitivity is utterly

significant in the realistic application of optical temperature sensing materials as vital parameter to evaluate the performance of sensor, which consists of absolute sensitivity (S_a) and relative sensitivity (S_r). The significant research parameter S_a and S_r can be calculated by the following Eqs. 4 and 5: [40, 41]

$$S_r = \frac{1}{FIR} \cdot \frac{dFIR}{dT} = \frac{\Delta E}{K_B T^2} \qquad (4)$$

$$S_a = \frac{dFIR}{dT} = B \frac{\Delta E}{K_B T^2} \exp\left(-\frac{\Delta E}{K_B T}\right) \qquad (5)$$

And the relationship among sensitivity (S_r and S_a) and T are shown in Fig. 5d–f. With the increase of temperature, the maximum values of S_r of $LiYb_{1-x}Mo_2O_8:xLn^{3+}$ are 1.16% K^{-1} ($^2H_{11/2}/^4S_{3/2} \rightarrow {}^4I_{15/2}$ of Er^{3+}), 0.25% K^{-1} ($^5F_5 \rightarrow {}^5I_8$ of Ho^{3+}), and 0.51% K^{-1} ($^1G_{4(1)}/^1G_{4(2)} \rightarrow {}^3H_6$ of Tm^{3+}), respectively. In addition, the S_a value of Er^{3+}-doped phosphor will reach the maximum (1.08% K^{-1}) at 475 K, while the maximum values of S_a of $LiYb_{0.99}Mo_2O_8:0.01Ho^{3+}$ and $LiYb_{0.99}Mo_2O_8:0.01Tm^{3+}$ are 0.16% K^{-1} and 0.14% K^{-1}. Some optical temperature sensing data of Ln^{3+}-doped samples are presented in Table 4. It can be clearly observed that the maximum values of S_r of

Fig. 5 **a** Lognormal plot of the FIR of $I_{532\ nm}/I_{553\ nm}$ as a function of the reciprocal of temperature about $LiYb_{0.95}Mo_2O_8:0.05Er^{3+}$. **b** Lognormal plot of the FIR of $I_{643\ nm}/I_{662\ nm}$ as a function of the reciprocal of temperature about $LiYb_{0.99}Mo_2O_8:0.01Ho^{3+}$. **c** Lognormal plot of the FIR of $I_{486\ nm}/I_{477\ nm}$ as a function of

the reciprocal of temperature about $LiYb_{0.99}Mo_2O_8:0.01Tm^{3+}$. The relationship between sensitivity and temperature about **d** $LiYb_{0.95}Mo_2O_8:0.05Er^{3+}$, **e** $LiYb_{0.99}Mo_2O_8:0.01Ho^{3+}$, and **f** $LiYb_{0.99}Mo_2O_8:0.01Tm^{3+}$

Table 4 Comparative list for maximum sensitivity values of different temperature sensing materials

RE ion(s)	Matrix	Transitions	Temperature range (K)	Sr_{max} (K^{-1})	References
Yb^{3+}/Er^{3+}	YPO_4	$^2H_{11/2}/^4S_{3/2} \rightarrow {}^4I_{15/2}$	313–573	0.27%	[8]
Yb^{3+}/Er^{3+}	$Ba_2TiGe_2O_8$	$^2H_{11/2}/^4S_{3/2} \rightarrow {}^4I_{15/2}$	333–573	0.59%	[6]
Yb^{3+}/Er^{3+}	$Ba_5Gd_8Zn_4O_{21}$	$^2H_{11/2}/^4S_{3/2} \rightarrow {}^4I_{15/2}$	200–500	0.32%	[26]
Yb^{3+}/Er^{3+}	$CaLa_2ZnO_5$	$^2H_{11/2}/^4S_{3/2} \rightarrow {}^4I_{15/2}$	298–513	0.59%	[40]
Yb^{3+}/Ho^{3+}	$Ba_2TiGe_2O_8$	$^5F_5 \rightarrow {}^5I_8$	300–550	0.16%	[6]
Yb^{3+}/Ho^{3+}	$KLu(WO_4)_2$	$^5F_5 \rightarrow {}^5I_8$	297–673	0.38%	[10]
Yb^{3+}/Tm^{3+}	Y_2O_3	$^1G_{4(2)}/^1G_{4(1)} \rightarrow {}^3H_6$	303–753	0.35%	[36]
Yb^{3+}/Tm^{3+}	$Na_2Y_2B_2O_7$	$^1G_{4(2)}/^1G_{4(1)} \rightarrow {}^3H_6$	300–625	0.45%	[32]
Yb^{3+}/Er^{3+}	$LiYbMo_2O_8$	$^2H_{11/2}/^4S_{3/2} \rightarrow {}^4I_{15/2}$	300–500	1.16%	This work
Yb^{3+}/Ho^{3+}	$LiYbMo_2O_8$	$^5F_5 \rightarrow {}^5I_8$	301–451	0.25%	This work
Yb^{3+}/Tm^{3+}	$LiYbMo_2O_8$	$^1G_{4(2)}/^1G_{4(1)} \rightarrow {}^3H_6$	300–480	0.51%	This work

$LiYb_{1-x}Mo_2O_8:xLn^{3+}$ phosphors possess the higher status by comparing the reported literatures, which are depended on the same thermal coupling energy level. The changing law of temperature sensitivity (S_r and S_a) under distinct temperatures indicates the practicability of $LiYb_{1-x}Mo_2O_8:xLn^{3+}$ in the field of temperature sensing.

4 Conclusions

In summary, a series of $LiYb_{1-x}Mo_2O_8:xLn^{3+}$ (Ln = Er, Ho, Tm) phosphors were successfully synthesized by traditional high-temperature solid-state method. The XRD pattern from Rietveld refinement indicated that $LiYbMo_2O_8$ was the double molybdates with a monoclinic structure ($I4_1/a$). The UC luminescence properties of $LiYb_{1-x}Mo_2O_8:xLn^{3+}$ are investigated, all emission processes about Ho^{3+} ions and Er^{3+} ions are two-photon processes and the blue emission process about Tm^{3+} ions is a combination of two-photon process and three-photon process. Moreover, the temperature-dependent properties investigations based on FIR technology were estimated, which give powerful evidence for the potential application in optical temperature sensing.

Acknowledgements

References

1. F. Cheng, Z. Xia, X. Jing, Z. Wang, Li/Ag ratio dependent structure and upconversion photoluminescence of $Li_xAg_{1-x}Yb_{0.99}(MoO_4)_2:0.01Er^{3+}$ phosphors. Phys. Chem. Chem. Phys. **17**, 3689–3696 (2015)

2. H. Dong, L. Sun, C. Yan, Energy transfer in lanthanide upconversion studies for extended optical applications. Chem. Soc. Rev. **44**, 1608–1634 (2015)

3. T. Li, C. Guo, Y. Wu, L. Li, J.H. Jeong, Green upconversion luminescence in Yb^{3+}/Er^{3+} co-doped $ALn(MoO_4)_2$ (A=Li, Na and K; Ln=La, Gd and Y). J. Alloys Compd. **540**, 107–112 (2012)

4. X. Gao, D. Xu, J. Du, J. Li, Z. Yang, J. Sun, Research of optical absorption and luminescence spectra of double-perovskite calcium tungstate co-doped with Yb^{3+}/Ho^{3+}. J. Mater. Sci.: Mater. Electron. **29**, 1146–1152 (2017)

5. T. Jiang, Y. Tian, M. Xing, Y. Fu, X. Yin, H. Wang, X. Feng, X. Luo, Research on the photoluminescence and up-conversion luminescence properties of $Y_2Mo_4O_{15}$: Yb, Ho under 454 and 980 nm excitation. Mater. Res. Bull. **98**, 328–334 (2018)

6. B. Hou, M. Jia, P. Li, G. Liu, Z. Sun, Z. Fu, Multifunctional optical thermometry based on the rare-earth-ions-doped up-/down-conversion $Ba_2TiGe_2O_8$: Ln (Ln = $E^{u3+}/E^{r3+}/H^{o3+}/Y^{b3+}$) phosphors. Inorg. Chem. **58**, 7939–7946 (2019)

7. N. Zhang, M.S. Molokeev, Q. Liu, Z. Xia, Pure red upconversion luminescence and optical thermometry of Er^{3+} doped sensitizer-rich $SrYbInO_4$ phosphors. J. Mater. Chem. C **6**, 7361–7366 (2018)

8. X. Zhang, Z. Fu, Z. Sun, G. Liu, J.H. Jeong, Z. Wu, Temperature-induced phase transition and temperature sensing behavior in Yb^{3+} sensitized Er^{3+} doped YPO_4 phosphors. Opt. Mater. **60**, 526–532 (2016)

9. J. Liao, Q. Wang, L. Kong, Z. Ming, Y. Wang, Y. Li, L. Che, Effect of Yb^{3+} concentration on tunable upconversion luminescence and optically temperature sensing behavior in Gd_2TiO_5:Yb^{3+}/Er^{3+} phosphors. Opt. Mater. **75**, 841–849 (2018)

10. O.A. Savchuk, J.J. Carvajal, M.C. Pujol, E.W. Barrera, J. Massons, M. Aguilo, F. Diaz, Ho, Yb:KLu(W_O4)2 nanoparticles: a versatile material for multiple thermal sensing purposes by luminescent thermometry. J. Phys. Chem. C **119**, 18546–18558 (2015)

11. J. Zhang, Y. Zhang, X. Jiang, Investigations on upconversion luminescence of $K_3Y(PO_4)_2$:Yb^{3+}-Er^{3+}/Ho^{3+}/Tm^{3+} phosphors for optical temperature sensing. J. Alloys Compd. **748**, 438–445 (2018)

12. Z. Fu, T. Sheng, Z. Wu, Y. Yu, T. Cui, A novel and tunable upconversion luminescent material GdPO4: Yb^{3+}, Ln^{3+} (Ln=Er, Tm, Ho). Mater. Res. Bull. **56**, 138–142 (2014)

13. N. Wang, Z. Fu, Y. Wei, T. Sheng, Investigation for the upconversion luminescence and temperature sensing mechanism based on BiPO4: Yb^{3+}, RE^{3+} (RE^{3+} = Ho^{3+}, Er^{3+} and Tm^{3+}). J. Alloys Compd. **772**, 371–380 (2019)

14. V. Volkov, C. Cascales, A. Kling, C. Zaldo, Growth, structure, and evaluation of laser properties of LiYb(MoO_4)2 single crystal. Chem. Mater. **17**, 291–300 (2005)

15. X. Qiao, H.J. Seo, Tunable white upconversion luminescence in Ho^{3+}/Tm^{3+} co-doped Yb-based LiYb(MoO_4)2. Mater. Lett. **105**, 166–168 (2013)

16. R. Cao, C. Liao, F. Xiao, G. Zheng, W. Hu, Y. Guo, Y. Ye, Emission enhancement of $LiLaMo_2O_8$:Eu^{3+} phosphor by co-doping with Bi^{3+} and Sm^{3+} ions. Dyes Pigm. **149**, 574–580 (2018)

17. Bruker AXS TOPAS V4: General profile and structure analysis software for powder diffraction data—User's Manual, Bruker AXS, Karlsruhe, Germany, 2008

18. F. Cheng, Z. Xia, M.S. Molokeev, X. Jing, Effects of composition modulation on the luminescence properties of Eu^{3+} doped $Li_{1-x}Ag_xLu(MoO4)_2$ solid-solution phosphors. Dalton Trans. **44**, 18078–18089 (2015)

19. S. Balabhadra, M.L. Debasu, C.D.S. Brites, R.A.S. Ferreira, L.D. Carlos, Upconverting nanoparticles working as primary thermometers in different media. J. Phys. Chem. C **121**, 13962–13968 (2017)

20. Y. Wei, C. Su, H. Zhang, J. Shao, Z. Fu, Color-tunable upconversion emission from Yb^{3+}/Er^{3+}/Tm^{3+}/Ho^{3+} codoped KY(MoO_4)2 microcrystals based on energy transfer. Ceram. Int. **42**, 4642–4647 (2016)

21. Z. Zhang, C. Guo, H. Suo, X. Zhao, N. Zhang, T. Li, Thermometry and up-conversion luminescence of Yb^{3+}-Er^{3+} co-doped $Na_2Ln_2Ti_3O_{10}$ (Ln = Gd, La) phosphors. Phys. Chem. Chem. Phys. **18**, 18828–18834 (2016)

22. X. Yu, F. Song, C. Zou, L. Luo, C. Ming, W. Wang, Z. Cheng, L. Han, T. Sun, J. Tian, Temperature dependence of luminescence behavior in Er^{3+}/Yb^{3+} co-doped transparent phosphate glass ceramics. Opt. Mater. **31**, 1645–1649 (2009)

23. A. Zhang, M. Jia, Z. Sun, G. Liu, Z. Fu, T. Sheng, P. Li, F. Lin, High concentration Eu^{3+}-doped NaYb(MoO_4)2 multifunctional material: thermometer and plant growth lamp matching phytochrome PR. J. Alloys Compd. **782**, 203–208 (2019)

24. H.K. Park, J.H. Oh, H. Kang, J. Zhang, Y.R. Do, Hybrid 2D photonic crystal-assisted $Lu_3Al_5O_{12}$: Ce ceramic-plate phosphor and free-standing red film phosphor for white LEDs with High Color-Rendering Index. ACS Appl. Mater. Interfaces **7**, 4549–4559 (2015)

25. T. Li, C. Guo, S. Zhou, C. Duan, M. Yin, Highly sensitive optical thermometry of Yb^{3+}-Er^{3+}codoped AgLa(MoO_4)2 green upconversion phosphor. J. Am. Ceram. Soc. **98**, 2812–2816 (2015)

26. H. Suo, C. Guo, T. Li, Broad-scope thermometry based on dual-color modulation up-conversion phosphor $Ba_5Gd_8Zn_4O_{21}$:Er^{3+}/Yb^{3+}. J. Phys. Chem. C **120**, 2914–2924 (2016)

27. Y. Wu, H. Suo, D. He, C. Guo, Highly sensitive up-conversion optical thermometry based on Yb^{3+} -Er^{3+} co-doped NaLa(MoO_4)2 green phosphors. Mater. Res. Bull. **106**, 14–18 (2018)

28. H. Zhang, J. Ye, X. Wang, S. Zhao, R. Lei, L. Huang, S. Xu, Highly reliable all-fiber temperature sensor based on the fluorescence intensity ratio (FIR) technique in Er^{3+}/Yb^{3+} co-doped $NaYF_4$ phosphors. J. Mater. Chem. C **7**, 15269–15275 (2019)

29. H. Suo, C. Guo, W. Wang, T. Li, C. Duan, M. Yin, Mechanism and stability of spectrally pure green up-conversion emission in Yb^{3+}/Ho^{3+} co-doped $Ba_5Gd_8Zn_4O_{21}$ phosphors. Dalton Trans. **45**, 2629–2636 (2016)

30. J. Li, T. Li, H. Suo, X. Zhao, C. Guo, Up-conversion emission color tuning in NaLa(MoO4)2: Nd3+/Yb3+/Ho3+ excited at 808 nm. Ceram. Int. **43**, 6333–6339 (2017)

31. M. Runowski, A. Bartkowiak, M. Majewska, I.R. Martín, S. Lis, Upconverting lanthanide doped fluoride $NaLuF_4$:Yb^{3+}-Er^{3+}-Ho^{3+} - optical sensor for multi-range fluorescence intensity ratio (FIR) thermometry in visible and NIR regions. J. Lumin. **201**, 104–109 (2018)

32. A.K. Soni, R. Dey, V.K. Rai, Stark sublevels in Tm^{3+}–Yb^{3+} codoped $Na_2Y_2B_2O_7$ nanophosphor for multifunctional applications. RSC Adv. **5**, 34999–35009 (2015)

33. X. Tu, J. Xu, M. Li, T. Xie, R. Lei, H. Wang, S. Xu, Color-tunable upconversion luminescence and temperature sensing behavior of Tm^{3+}/Yb^{3+} codoped $Y_2Ti_2O_7$ phosphors. Mater. Res. Bull. **112**, 77–83 (2019)

34. J. Zhang, Y. Chen, G. Chen, Investigation of dopant concentration and excitation power on sensitivities of $Y_{4.67}(SiO_4)_3O:Yb^{3+},Er^{3+}$ upconversion phosphors for optical thermometer. Opt. Laser Technol. **120**, 105747 (2019)

35. H. Suo, C. Guo, Z. Yang, S. Zhou, C. Duan, M. Yin, Thermometric and optical heating Bi-functional properties of upconversion phosphor $Ba_5Gd_8Zn_4O_{21}:Yb^{3+}/Tm^{3+}$. J. Mater. Chem. C **3**, 7379–7385 (2015)

36. D. Li, Y. Wang, X. Zhang, K. Yang, L. Liu, Y. Song, Optical temperature sensor through infrared excited blue upconversion emission in Tm^{3+}/Yb^{3+} codoped Y_2O_3. Opt. Commun. **285**, 1925–1928 (2012)

37. W. Liu, X. Wang, Q. Zhu, X. Li, X. Sun, J. Li, Upconversion luminescence and favorable temperature sensing performance of eulytite-type $Sr_3Y(PO_4)_3:Yb^{3+}/Ln^{3+}$ phosphors (Ln=Ho, Er, Tm). Sci. Technol. Adv. Mater. **20**, 949–963 (2019)

38. J. Zhang, X. Jiang, Z. Hua, Investigation on upconversion luminescence and optical temperature sensing behavior for $Ba_2Gd_2Si_4O_{13}:Yb^{3+}-Er^{3+}/Ho^{3+}/Tm^{3+}$ phosphors. Ind. Eng. Chem. Res. **57**, 7507–7515 (2018)

39. J. Zhang, C. Jin, Electronic structure, upconversion luminescence and optical temperature sensing behavior of $Yb^{3+}-Er^{3+}/Ho^{3+}$ doped $NaLaMgWO_6$. J. Alloys Compd. **783**, 84–94 (2019)

40. L. Li, C. Guo, S. Jiang, D.K. Agrawal, T. Li, Green upconversion luminescence of $Yb^{3+}-Er^{3+}$ co-doped $CaLa_2ZnO_5$ for optically temperature sensing. RSC Adv. **4**, 6391–6396 (2014)

41. H. Li, Y. Zhang, L. Shao, P. Yuan, X. Xia, Influence of pump power and doping concentration for optical temperature sensing based on $BaZrO_3:Yb^{3+}/Ho^{3+}$ ceramics. J. Lumin. **192**, 999–1003 (2017)